Solar Energy 171 (2018) 871–875

Contents lists available at ScienceDirect

Solar Energy

journal homepage: www.elsevier.com/locate/solener

Theoretical study of electronic structure and optical properties of tin doped CuS counter electrode for dye-sensitized solar cells

Jianbo Yin[a,b,*], Xuefeng Lu[b]

[a] State Key Laboratory of Advanced Processing and Recycling of Non–ferrous Metals, Lanzhou University of Technology, Lanzhou 730050, China
[b] School of Material Science and Engineering, Lanzhou University of Technology, Lanzhou 730050, China

ARTICLE INFO

Keywords:
First principles
Counter electrode
Electronic structure
Optical properties

ABSTRACT

In order to study whether tin doped CuS could be used as counter electrodes for dye-sensitized solar cells, first-principles were used to calculate the electronic structure and optical properties of it. The calculated results show that tin ions can substitute two different kinds of copper ions in the supercell of CuS, and they demonstrate different properties. The calculated results of electronic structure indicate that the introduction of tin ions change the conductive properties of CuS counter electrode. The calculated results of optical properties indicate that the introduction of tin ions change the optical properties of CuS counter electrode, and tin doped CuS could be excellent counter electrodes for dye-sensitized solar cells.

1. Introduction

Over the past few decades, great progress has been made in optoelectronic materials and devices (Ahmad et al., 2017; Zhang et al., 2017; Shi et al., 2017; Wang et al., 2017; Lu et al., 2017). Dye-sensitized solar cells (DSSC), which are electrochemical devices converting solar energy into electricity, could offer a promising solution to utilize renewable energy for substituting traditional fossl fuels (Nagarajan et al., 2017; Ahmad et al., 2017; Taleb et al., 2016). DSSC typically consist of three parts: a photoanode, an electrolyte and a counter electrode (CE). Among these three parts, CE plays a very significant role in collecting electric current from an external circuit and promoting the reduction reaction of redox couple. Thus, CE directly affects the photoelectric conversion efficiency of a DSSC (Wei et al., 2016; Duan et al., 2016). So far, various materials have been explored to prepare CE, such as Pt CE (Hsieh et al., 2015; Chen et al., 2017), conducting polymers (Seo et al., 2016; Li et al., 2016), carbonaceous materials (Du et al., 2016; Liu et al., 2016); alloys (Qian et al., 2016) and inorganic compounds (Gopi et al., 2016; Liu et al., 2016). Pt has been considered as a preferred CE material for its superior electrical conductivity and electrocatalytic ability; conducting polymers have been studied intensively mainly due to their easy synthesis and cost effectiveness; carbonaceous materials can be used for potential CE catalysts mainly because they display a low sheet resistance and good corrosion resistance; alloys have attracted considerable interest recently years mainly due to the simple preparation process, low cost and excellent catalytic properties. Among these CE materials, inorganic compounds are preferred by more and more researchers due to their stable properties, excellent electrical conductivity and high catalytic activity. As available inorganic compounds, metal sulfides (such as CuS, $NiCo_2S_4$ and $CoNi_2S_4$) are preferred by more and more researchers for their excellent conductivity and easily synthesized property (Lu et al., 2016; Palve et al., 2017; Krishnapriya et al., 2017; Chen et al., 2015).

To date, the investigations show that CuS has a hexagonal phase and hole-conduction at room temperature (Lv et al., 2017). CuS has recently become widely studied electrode materials for DSSC, QDSSC (quantum dot-sensitized solar cells) and supercapacitors with excellent results. Xuemin Shuai et al. prepared CuS low-cost counter electrodes for DSSC and it demonstrated excellent performance in DSSC (Ramamoorthy and Rajendran, 2017). Youngson Choe et al. prepared CuS counter electrode for QDSSC and it showed that the CuS CE exhibited an inferior charge transfer resistance of only 2.93 Ω, which was 33 times lesser than that of the Pt CE (Sunesh et al., 2017). This replacement of Pt by CuS CE provides a low-cost DSSC device due to the Pt catalytic CE accounts for more than 50% of the whole cost.

These performance of CuS CE across similar applications has been mainly attributed to their excellent conductivity. Though CuS CE has been heavily investigated by experiments (Buatong et al., 2017; Hessein et al., 2017; Zhang et al., 2018; Liu et al., 2017); the influence of impurities on structure and properties has still poorly studied. Therefore,

* Corresponding author at: State Key Laboratory of Advanced Processing and Recycling of Non–ferrous Metals, Lanzhou University of Technology, Lanzhou 730050, China.
E-mail address: jianbery@163.com (J. Yin).

https://doi.org/10.1016/j.solener.2018.07.037
Received 20 April 2018; Received in revised form 9 July 2018; Accepted 13 July 2018
Available online 25 July 2018
0038-092X/

it is necessary to calculate the electronic structures, optical and electrical properties of doped CuS CE via theoretical simulation study, which could also offer internal microstructure change and calculate different properties of CuS CE. In this work, First principles are adopted to study the electronic structures, optical and electrical properties of tin doped CuS. We introduce tin impurities in the CuS crystal cell to complete simulation because CuS coatings are usually on FTO (Fluorine-doped tin oxide) coating of conductive glass in experiments (Diwate et al., 2018; Bhat et al., 2017), and the study results show that tin changes the optical properties of CuS CE.

2. Computational details

First principles simulation of CuS was implemented with the Cambridge Serial Total Energy Package module (CASTP) of Material Studio. The simulation adopted the super cell of hexagonal phase CuS which consisted 24 ions, including 12 copper atoms and 12 sulfur atoms, respectively. The core electrons were optimized by normal-conserving pseudopotential and local density approximation (LDA) functionals. And the PBE method was applied as the exchange-correlation effects of valence electrons. The Monkhorste-Pack scheme k-points grid sampling was set as 8 × 8 × 2 for the irreducible Brillouin zone. The energy cutoff was chosen 440 eV. The electronic configurations are $3d^{10}4s^1$ for copper, $3s^23p^4$ for sulfur and $5s^25p^2$ for tin, respectively.

3. Results and discussions

The space group of CuS is $P6_3/mmc$ (space group #227) which is a hexagonal crystal structure and the lattice constants are a = b = 3.794 Å and c = 16.341 Å. The calculation adopts the super cell of hexagonal phase CuS which contains 24 atoms, including 12 copper atoms and 12 sulfur atoms, respectively. The norm-conserving pseudopotentials are choosen for the calculation results are more consistent with the experimental results than ultrasoft pseudopotentials (Lv et al., 2017; Ramamoorthy and Rajendran, 2017). The relaxed lattice constants of hexagonal phase CuS are a = b = 3.776 Å, and c = 16.291 Å and α = β = γ = 90°, γ = 120° which are consistent with the experiment results (Ramamoorthy and Rajendran, 2017). The relaxed unit cell of pure hexagonal phase CuS is shown in Fig. 1. The Wyckoff position of Cu (No.1) cation is (0.667, 0.333, 0.250) and Cu (No.2) is (0.333, 0.667, 0.1073), while that of anion S (No.1) is (0.333, 0.667, 0.25) and S (No.2) is (0, 0, 0.0634).

The band structure and density of state (DOS) of hexagonal phase CuS along the high symmetry directions in the Brillouin zone are calculated based on the LDA and GGA functionals because only these two functionals could be used to calculate the electronic structure of conductors, but the results show that there is little difference between the two methods. Therefore, we only exhibit the calculated results of LDA functional here. The calculated results of electronic structure by LDA functional are shown in Figs. 2 and 3, respectively. Fig. 2a shows the band structure model of pure hexagonal phase CuS, and Fermi level indicates by a red line is set to zero. Fermi level intersecting with several energy bands indicate that pure hexagonal phase CuS is a conductor, and the partial density of states (PDOS) shown in Fig. 3a indicate that there are antibonding states of S-p at Fermi level (0 eV), showing S-p is involved in the electrical conduction process of pure hexagonal phase CuS. Fig. 2(b) and (c) show the band gap models of hexagonal phase CuS with tin substituting Cu (No.1) and Cu (No.2), respectively. The impurity levels bend across the Fermi level, which shows the conductivity is changed. It can be seen from the PDOS of Fig. 3(b) and (c) that the impurity levels are Sn-s and Sn-p orbitals, respectively. Therefore, the calculation results show that the introduction of tin can change the conductivity of hexagonal phase CuS.

In order to obtain the detailed optical properties of tin doped CuS, the optical absorption coefficient and the reflectivity are calculated as shown in Fig. 4(a) and (b), respectively. From Fig. 4(a), it can be seen that the sharp optical absorption peak of pure CuS is at about the wavelength of 120 nm, and the absorption coefficient at the visible region (380–780 nm) is very small, which is about 2.5×10^4. But that of tin doped CuS become obviously larger than that of pure CuS in UV–visible region, and both the absorption coefficient of them are over the magnitude of 5.0×10^4. The results are similar with the reflectivity curves of Fig. 4(b), the maximum sharp peak of which are at the same range, indicating the maximum value of reflectivity is corresponding to that of absorption. In the visible region, the reflectivity of pure CuS is about 0.2, and it is smaller than that of tin doped CuS, the reflectivity value of which is about 0.4. Therefore, the calculated results indicate that the introduction tin impurities increase light absorption coefficients and reflectivity of CuS.

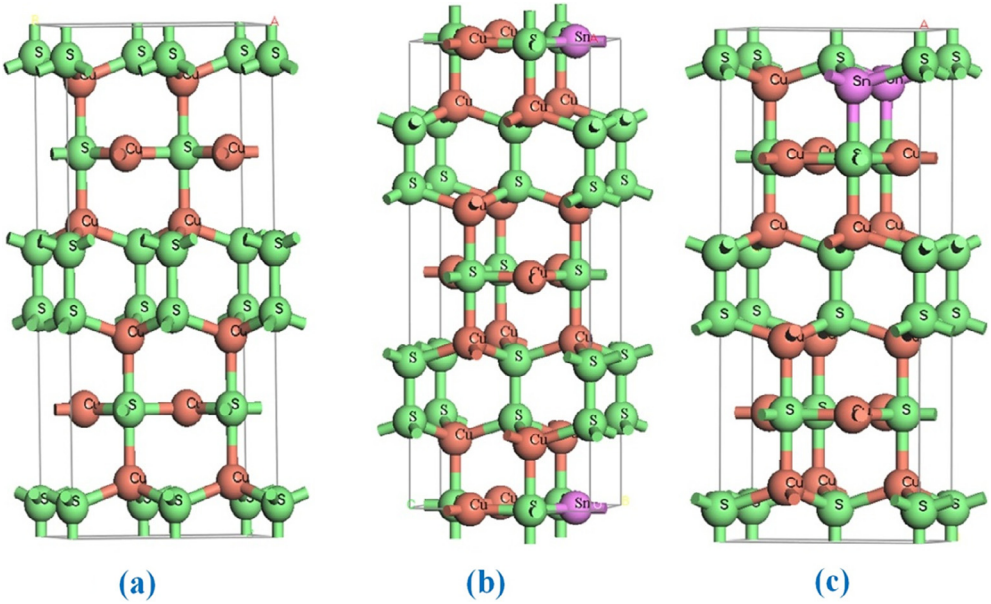

Fig. 1. Supercell of tin doped CuS. (a) supercell of pure hexagonal phase CuS; (b) supercell of hexagonal phase CuS the copper ion (No.1) of which is replaced by the tin ion; (c) supercell of hexagonal phase CuS the copper ion (No.2) of which is replaced by the tin ion.

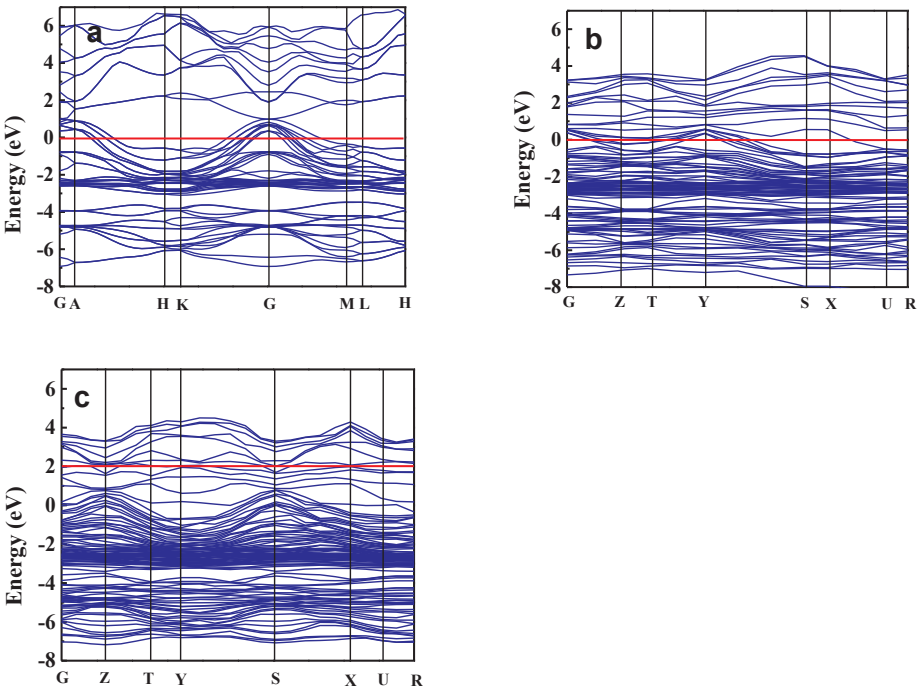

Fig. 2. The band structure maps of tin doped CuS. (a) the band structure maps of pure hexagonal phase CuS; (b) the band structure maps of hexagonal phase CuS the copper ion (No.1) of which is replaced by the tin ion; (c) the band structure maps of hexagonal phase CuS the copper ion (No.2) of which is replaced by the tin ion.

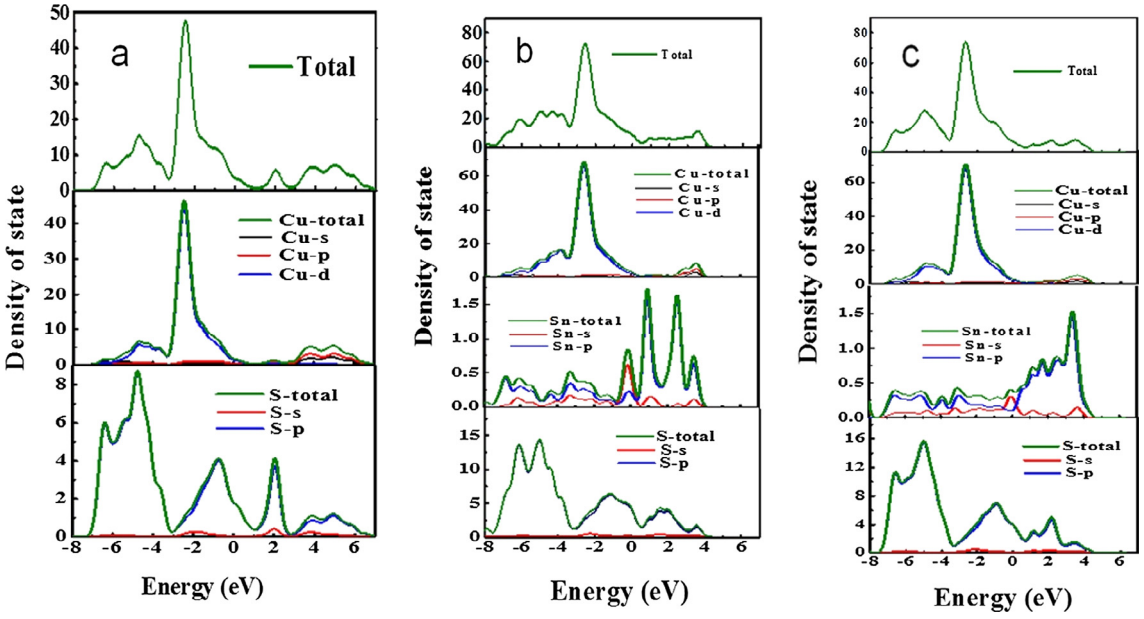

Fig. 3. Density of state maps of tin doped CuS. (a) density of state maps of pure hexagonal phase CuS; (b) density of state maps of hexagonal phase CuS the copper ion (No.1) of which is replaced by the tin ion; (c) density of state maps of hexagonal phase CuS the copper ion (No.2) of which is replaced by the tin ion.

Fig. 5(a) and (b) present the imaginary parts of dielectric coefficient and real parts of the optical conductivity for tin doped CuS, respectively. The dielectric property can be expressed by the complex permittivity $\varepsilon(\omega) = \varepsilon_1(\omega) + i\varepsilon_2(\omega)$. The imaginary part $\varepsilon_2(\omega)$ shows the power loss, which is an very important parameter of optical property. As can be seen from Fig. 5(a), the $\varepsilon_2(\omega)$ of pure CuS is low in visible region, the value of which is about 2.5. However, the $\varepsilon_2(\omega)$ of tin doped CuS is higher than that of pure CuS in visible region, the values of which are greater than 5, and they also have wide peaks in the whole visible region. As can be seen from Fig. 5(b) that the curve trend of optical conductivity spectra is somewhat different with that of dielectric coefficient spectra. All of the three curves have sharp peaks in UV region and also they decline slowly in visible region, but the values of tin doped CuS are obviously greater than that of pure CuS. Therefore, the calculated results show the introduction of tin impurities could increase the dielectric power loss and optical conductivity.

As one of the most important optical property parameter, the complex refractive index, which is determined by the wavelength of electromagnetic wave, is defined as $N(\omega) = n(\omega) + ik(\omega)$, where $n(\omega)$ is the refractive index and $k(\omega)$ is extinction coefficient, respectively. Fig. 6 shows $n(\omega)$ and $k(\omega)$ as functions of the optical wavelength for tin doped CuS, respectively. The variations of $n(\omega)$ and $k(\omega)$ in Fig. 6 are very similar to those of imaginary part $\varepsilon_2(\omega)$ of the dielectric function and the real part of dielectric coefficient in Fig. 6a,

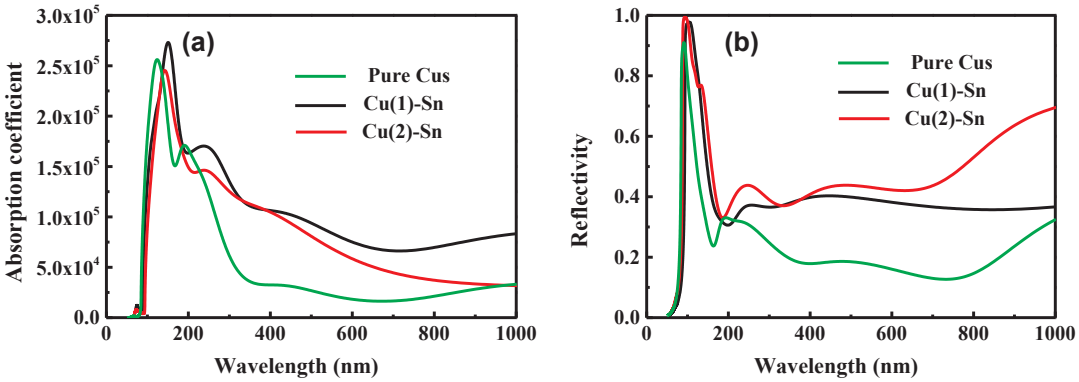

Fig. 4. Calculated absorption coefficients (a) and reflectivities (b) of tin doped CuS.

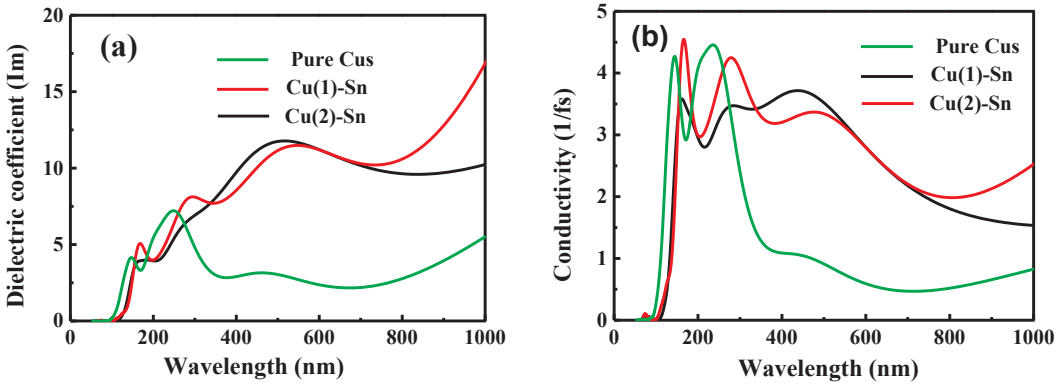

Fig. 5. Calculated imaginary parts $\varepsilon_2(\omega)$ of the dielectric function (a) and real parts of conductivity (b) for tin doped CuS.

respectively. For pure CuS, as the wavelength increases, n(ω) decreases slowly in the visible region, and the tin doped CuS of that is greater than that of pure CuS in visible region. The behaviors of k(ω) is slightly different with that of n(ω). In the visible region, both the curves of pure CuS and the tin substituting Cu (No.2) CuS is slowly increasing with the increasing of wavelength, but the tin substituting Cu (No.1) CuS is slowly decreasing with the increasing of wavelength, respectively. Therefore, the study results show that the introduction of tin impurities lead to refractive index and extinction coefficients curves of CuS increasing in visible region.

4. Conclusions

In this study, the electronic structures and optical properties of tin doped CuS were investigated by first-principles DFT calculations. The calculated results of electronic structures indicate that the introduction of tin changes the conductivity of CuS, and Sn-s and Sn-p are involved in the electrical conduction process. The calculated results of optical properties indicate that the introduction of tin ions has increased absorption coefficient and reflectivity of CuS, and the photoconductive study results indicate that tin doped CuS could be an excellent counter electrode.

Acknowledgement

This paper is supported by the Gansu Provincial Youth Science and Technology Fund Projects of China (1506RJYA093) and National Natural Science Foundations of China (Granted Nos. 51402142, 21301084 and 51662026).

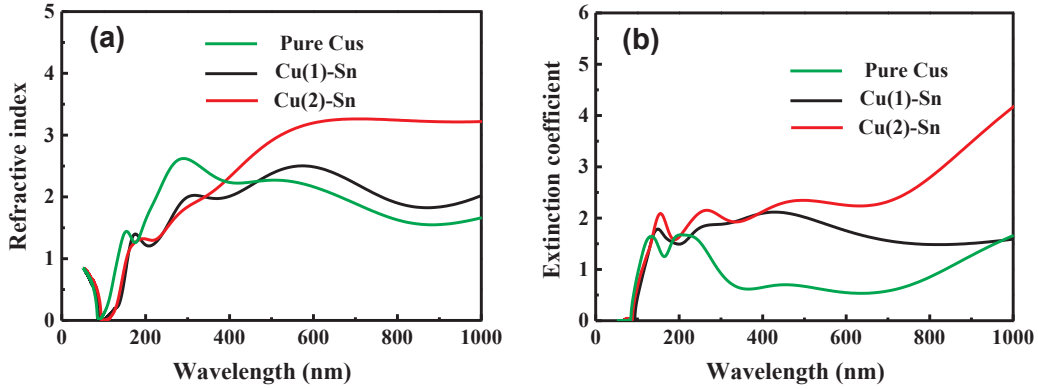

Fig. 6. Calculated n(ω) refractive indexes (a) and k(ω) extinction coefficients (b) for tin doped CuS.

References

Ahmad, M.S., Pandey, A.K., Rahim, N.A., 2017. Advancements in the development of TiO_2 photoanodes and its fabrication methods for dye sensitized solar cell (DSSC) applications. A review. Renew. Sustain. Energy Rev. 77, 89–108.

Ahmad, M.S., Pandey, A.K., Rahim, N.A., 2017. Advancements in the development of TiO_2 photoanodes and its fabrication methods for dye sensitized solar cell (DSSC) applications. A review. Renew. Sustain. Energy Rev. 77, 89–108.

Bhat, S.V., Dhanasekar, M., Rickey, K.M., Ruan, X., 2017. Facile in situ growth of nanostructured copper sulfide films directly on FTO coated glass substrates as efficient counter electrodes for quantum dot sensitized solar cells. Chem. Select 2 (33), 10736–10740.

Buatong, N., Tang, I.M., Pon-On, W., 2017. Fabrication of solar cells made with $CuInTe_{2-x}Se_x$ quantum dots sensitized hierarchical TiO_2 sphere having a CuS counter electrode: dependence on the Te/Se ratio. Mater. Lett. 199, 41–45.

Chen, R., Yang, C., Cai, W., et al., 2017. Use of platinum as the counter electrode to study the activity of nonprecious metal catalysts for the hydrogen evolution reaction. ACS Energy Lett. 2 (5), 1070–1075.

Chen, L., Zhou, Y., Dai, H., Yu, T., Liu, J., Zou, Z., 2015. One-step growth of $CoNi_2S_4$ nanoribbons on carbon fibers as platinum-free counter electrodes for fiber-shaped dye-sensitized solar cells with high performance: polymorph-dependent conversion efficiency. Nano Energy 11, 697–703.

Diwate, K., Rondia, S., Mayabadi, A., Rokade, A., Waykar, R., Borate, H., Funde, A., Shinde, M., Rajedra Prasad, M.B., Pathan, H., Jadkar, S., 2018. Chemical spray pyrolysis synthesis of covellite copper sulphide (CuS) thin films for economical counter electrode for DSSCs. J. Mater. Sci.: Mater. Electron. 29 (6), 4940–4947.

Du, Z., Pan, Z., Fabregat-Santiago, F., Zhao, K., Long, D., Zhang, H., Zhao, Y., Zhong, X., Yu, J.S., Bisquert, J., 2016. Carbon counter-electrode-based quantum-dot-sensitized solar cells with certified efficiency exceeding 11%. J. Phys. Chem. Lett. 7 (16), 3103–3111.

Duan, J., Tang, Q., Zhang, H., Meng, Y., Yu, L., Yang, P., 2016. Counter electrode electrocatalysts from one-dimensional coaxial alloy nanowires for efficient dye-sensitized solar cells. J. Power Sources 302, 361–368.

Gopi, C.V., Venkata-Haritha, M., Lee, Y.S., Kim, H.J., 2016. ZnO nanorods decorated with metal sulfides as stable and efficient counter-electrode materials for high-efficiency quantum dot-sensitized solar cells. J. Mater. Chem. A 4 (21), 8161–8171.

Hessein, A., Wang, F., Masai, H., Matsuda, K., Abd El-Moneim, A., 2017. Improving the stability of CdS quantum dot sensitized solar cell using highly efficient and porous CuS counter electrode. J. Renew. Sustain. Energy 9 (2), 023504.

Hsieh, T.Y., Wei, T.C., Zhai, P., Feng, S.P., Ikegami, M., Miyasaka, T., 2015. A room-temperature process for fabricating a nano-Pt counter electrode on a plastic substrate for efficient dye-sensitized cells. J. Power Sources 283, 351–357.

Krishnapriya, R., Praneetha, S., Rabel, A.M., Murugan, A.V., 2017. Energy efficient, one-step microwave-solvothermal synthesis of a highly electro-catalytic thiospinel $NiCo_2S_4$/graphene nanohybrid as a novel sustainable counter electrode material for Pt-free dye-sensitized solar cells. J. Mater. Chem. C 5 (12), 3146–3155.

Li, R., Tang, Q., Yu, L., Yan, X., Zhang, Z., Yang, P., 2016. Counter electrodes from conducting polymer intercalated graphene for dye-sensitized solar cells. J. Power Sources 309, 231–237.

Liu, J., Li, C., Zhao, Y., Wei, A., Liu, Z., 2016. Synthesis of $NiCo_2S_4$ nanowire arrays through ion exchange reaction and their application in Pt-free counter-electrode. Mater. Lett. 166, 154–157.

Liu, Z., Sun, B., Shi, T., Tang, Z., Liao, G., 2016. Enhanced photovoltaic performance and stability of carbon counter electrode based perovskite solar cells encapsulated by PDMS. J. Mater. Chem. A 4 (27), 10700–10709.

Liu, I.P., Teng, H., Lee, Y.L., 2017. Highly electrocatalytic carbon black/copper sulfide composite counter electrodes fabricated by a facile method for quantum-dot-sensitized solar cells. J. Mater. Chem. A 5 (44), 23146–23157.

Lu, X., Gao, X., Li, C., Ren, J., Guo, X., La, P., 2017. Electronic structure and optical properties of doped gallium phosphide: a first-principles simulation. Phys. Lett. A 381 (35), 2986–2992.

Lu, M.N., Lin, J.Y., Wei, T.C., 2016. Exploring the main function of reduced graphene oxide nano-flakes in a nickel cobalt sulfide counter electrode for dye-sensitized solar cell. J. Power Sources 332, 281–289.

Lv, Z., Cui, H., Huang, H., Li, X., Wang, H., Ji, G., 2017. Study of the electronic, bonding, elastic and acoustic properties of covellite via first principles. J. Alloy. Compd. 692, 440–447.

Nagarajan, B., Kushwaha, S., Elumalai, R., Mandal, S., Ramanujam, K., Raghavachari, D., 2017. Novel ethynyl-pyrene substituted phenothiazine based metal free organic dyes in DSSC with 12% conversion efficiency. J. Mater. Chem. A 5 (21), 10289–10300.

Palve, B.M., Kadam, V.S., Jagtap, C.V., Pathan, H.M., 2017. A simple chemical route to synthesis the CuSe and CuS counter electrodes for titanium oxide based quantum dot solar cells. J. Mater. Sci.: Mater. Electron. 28 (19), 14394–14401.

Qian, Y., Niehoff, P., Börner, M., Grützke, M., Mönnighoff, X., Behrends, P., Nowaka, S., Winter, M., Schappacher, F.M., 2016. Influence of electrolyte additives on the cathode electrolyte interphase (CEI) formation on $LiNi_{1/3}Mn_{1/3}Co_{1/3}O_2$ in half cells with Li metal counter electrode. J. Power Sources 329, 31–40.

Ramamoorthy, C., Rajendran, V., 2017. Synthesis and characterization of CuS nanostructures: structural, optical, electrochemical and photocatalytic activity by the hydro/solvothermal process. Int. J. Hydrogen Energy 42 (42), 26454–26463.

Seo, H., Son, M.K., Itagaki, N., Koga, K., Shiratani, M., 2016. Polymer counter electrode of poly (3, 4-ethylenedioxythiophene): Poly (4-styrenesulfonate) containing TiO_2 nanoparticles for dye-sensitized solar cells. J. Power Sources 307, 25–30.

Shi, G., Wang, Y., Zhang, F., Zhang, B., Yang, Z., Hou, X., Pan, S., Poeppelmeier, K.R., 2017. Finding the next deep-ultraviolet nonlinear optical material: NH4B4O6F. J. Am. Chem. Soc. 139 (31), 10645–10648.

Sunesh, C.D., Gopi, C.V., Muthalif, M.P.A., Kim, H.J., Choe, Y., 2017. Improving the efficiency of quantum-dot-sensitized solar cells by optimizing the growth time of the CuS counter electrode. Appl. Surf. Sci. 416, 446–453.

Taleb, A., Mesguich, F., Hérissan, A., Colbeau-Justin, C., Yanpeng, X., Dubot, P., 2016. Optimized TiO_2 nanoparticle packing for DSSC photovoltaic applications. Sol. Energy Mater. Sol. Cells 148, 52–59.

Wang, X., Wang, Y., Zhang, B., Zhang, F., Yang, Z., Pan, S., 2017. CsB4O6F: a congruent-melting deep-ultraviolet nonlinear optical material by combining superior functional units. Angew. Chem. 129 (45), 14307–14311.

Wei, W., Sun, K., Hu, Y.H., 2016. An efficient counter electrode material for dye-sensitized solar cells—flower-structured 1T metallic phase MoS_2. J. Mater. Chem. A 4 (32), 12398–12401.

Zhang, X., Lin, Y., Wu, J., Fang, B., Zeng, J., 2018. Improved performance of CdSe/CdS co-sensitized solar cells adopting efficient CuS counter electrode modified by PbS film using SILAR method. Opt. Commun. 412, 186–190.

Zhang, B., Shi, G., Yang, Z., Zhang, F., Pan, S., 2017. Fluorooxoborates: beryllium-free deep-ultraviolet nonlinear optical materials without layered growth. Angew. Chem. Int. Ed. 56 (14), 3916–3919.